Journal of Physics and Chemistry of Solids 73 (2012) 1111–1115

Contents lists available at SciVerse ScienceDirect

Journal of Physics and Chemistry of Solids

journal homepage: www.elsevier.com/locate/jpcs

ZnO-based spinels grown by electrodeposition

M. Tortosa [a], F.J. Manjón [a,b], M. Mollar [a], B. Marí [a,*]

[a] Institut de Disseny i Fabricació, Universitat Politècnica de València, E-46022 València, Spain
[b] MALTA Consolider Team, Spain

ARTICLE INFO

Article history:
Received 18 November 2011
Accepted 9 April 2012
Available online 11 May 2012

Keywords:
A. Thin solid films
A. Oxides
C. X-ray diffraction
C. Raman spectroscopy
D. Crystal structure

ABSTRACT

We report on the synthesis of thin films of $ZnCo_2O_4$ and $ZnMn_2O_4$ spinels, as well as pure Co_3O_4 and Mn_3O_4 spinels, by means of electrodeposition. Spinel thin films have been analyzed by energy dispersive spectroscopy, X-ray diffraction, and Raman spectroscopy. We show that under determined deposition conditions the initial wurtzite structure of Co- and Mn-doped ZnO develops into spinel structures when the Co and Mn concentration in the films is above the solubility limit of these ions in the typical ZnO-wurtzite structure.

1. Introduction

Spinel oxides have a general formula $A^{II}B^{III}_2O_4$ in which A is a small divalent metal with tetrahedral coordination and B is a large trivalent metal with octahedral coordination. It is known that spinels containing transition metal ions can act as efficient catalysts in a number of heterogeneous chemical processes, such as CO oxidation [1], catalytic combustion of hydrocarbons [2] or selective oxidation and reduction of several organic molecules [3–5]. They can also be used as gas sensors attending the growing demand for monitoring toxic and harmful gases [6] and also in Li-ion batteries [7,8].

Spinels are known to crystallize in either cubic (Fd-3m) or tetragonal ($I4_1/amd$) structures. The tetragonal spinel structure results from a distortion of the cubic spinel structure due to the deformation of octahedra as a result of Jahn–Teller interactions. In particular, Co_3O_4 ($Co^{2+}Co^{3+}_2O_4$) is a pure cubic spinel [9] while Mn_3O_4 ($Mn^{2+}Mn^{3+}_2O_4$) is a tetragonal spinel due to the presence of Jahn–Teller Mn^{3+} ions in octahedral sites [10]. Spinels are complex structures because they have unoccupied cation sites in the unit cell that lead to intrinsic disorder, called inversion, in which cations at tetrahedral and octahedral sites interchange their respective positions. Few vibrational studies of the spinel structure are reported in the literature because AO_4 and BO_6 polyhedra are very interrelated and it is difficult to interpret vibrational spectra in terms of single contribution from tetrahedral or octahedral units.

The most general method for preparing oxide spinels is the ceramic process that requires the solid-state reaction of a mixed powder of the parent metal binary oxides at rather high temperatures (usually higher than 1000 °C) during several days [11]. This method has several disadvantages such as inhomogeneities, lack of stoichiometric control and large particle size. These drawbacks can be avoided by synthesizing the materials using a solution-based method [12] where the mixing of different metal species occurs at a molecular level leading to the formation of polycrystalline homogeneous particles. In particular, $ZnCo_2O_4$ has been recently prepared by several solution-based methods including coprecipitation [13], hydrothermal synthesis [14], calcination of hydroxide or carbonate precursor mixtures [15], electrophoretic deposition [16], and sol–gel method [17].

In this paper we report the deposition of thin films of spinel oxides by means of cathodic electrodeposition. This low-cost technique presents many advantages including operation at low temperatures (lower than 100 °C) and at atmospheric pressure, the high homogeneity of the deposited films, the possibility of depositing large areas, and the direct monitoring of the deposited charge in order to control the film thickness. The main drawback is that a conducting substrate is required but this is not a problem for some applications of $ZnCo_2O_4$ like the use of this material as an oxygen (or chlorine) evolution electrode in solution [18–20]. We characterize the spinel thin films by means of Raman spectroscopy while most of the literature devoted to the spinel oxides dealt essentially with the infrared spectra of $A^{II}B^{III}_2O_4$ materials.

2. Experimental details

Ternary $Zn_xCo_yO_z$ and $Zn_xMn_yO_z$ films have been grown by electrodeposition onto ITO-coated glass substrate. The experimental setup used, basically is composed by a computer-controlled potentiostat/galvanostat and a classical three-electrode

* Corresponding author. Fax: +34 963 877 525.
E-mail address: bmari@fis.upv.es (B. Marí).

0022-3697/$ - see front matter © 2012 Elsevier Ltd. All rights reserved.
http://dx.doi.org/10.1016/j.jpcs.2012.04.002

electrochemical cell filled with a solution containing 0.1 M $KClO_4$ as supporting electrolyte and dissolved oxygen in a DMSO solution. Zn and Co chlorides are used as precursors: $ZnCl_2$, $CoCl_2$ and $MnCl_2$ in different concentrations. Pt and Ag/AgCl electrodes are used as counter electrode and reference electrode, respectively. The deposition potential was fixed at -0.9 V and the solution temperature was fixed at 900 °C by a thermostat. This experimental setup has been previously used for the growth of wurzite-type ZnO-based ternary thin films with a high transparency and homogeneity [21–24]. The chemical composition is determined by EDS, the structural characterization is obtained by high resolution diffractometer system "Rigaku Ultima IV" using a copper anticathode radiation (CuK_α, $\lambda = 1.542 \pm 0.002$ Å). Raman measurements have been excited with the 532 nm laser line using a LabRAM HR UV system with a Peltier-cooled CCD and resolution better than 2 cm^{-1}.

3. Results and discussion

Fig. 1 shows the EDS results where the molar fraction of the M (M=Co, Mn) ions in the ZnO films is represented as a function of the molar fraction of M in the initial solution. It is confirmed that the M-ions incorporate into the ZnO lattice. The different experimental points of Fig. 1 can be fitted with a Boltzmann function. Three different zones have been observed as a function of the initial molar fraction of the M ions in the solution: the first one (for values lower than 0.1 for Co and 0.3 for Mn), where the curve has small slope; the second zone (for values between 0.1 and 0.6 for Co and 0.3 and 0.6 for Mn), where the curve has a big slope; and finally, the third part for values larger than 0.6, where the curve has a small slope. The first zone is characterized by a small rate of incorporation of the M-ions into the wurtzite ZnO lattice and this leads to the formation of M-doped ZnO with concentrations below 10%. The second zone where the curve has a steep slope indicates a strong incorporation of M ions in the ZnO lattice well above the solubility limit of the M ions in the wurtzite lattice and it is the zone where the formation of ZnM_2O_4 spinels takes place. Finally, the third part is a flat zone where the concentration of the M ions in the films remains constant despite increasing the concentration in the initial solution. In this region occurs the formation of pure M_3O_4 spinels as we will show in the following paragraphs.

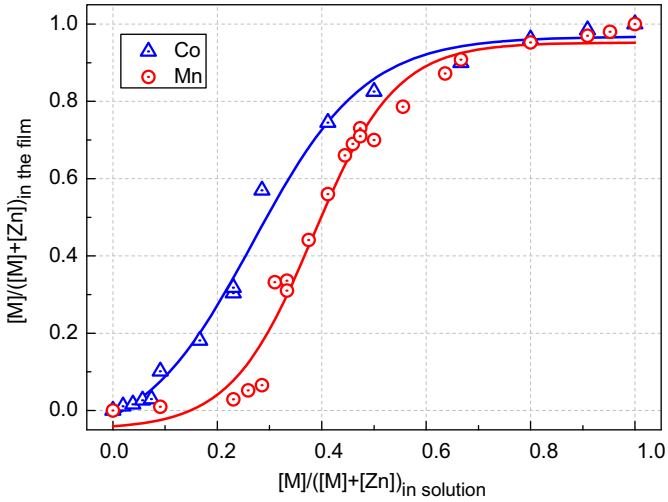

Fig. 1. M Fraction M/(M+Zn) in the deposited film as a function of the molar fraction M/(M+Zn) in the initial solution.

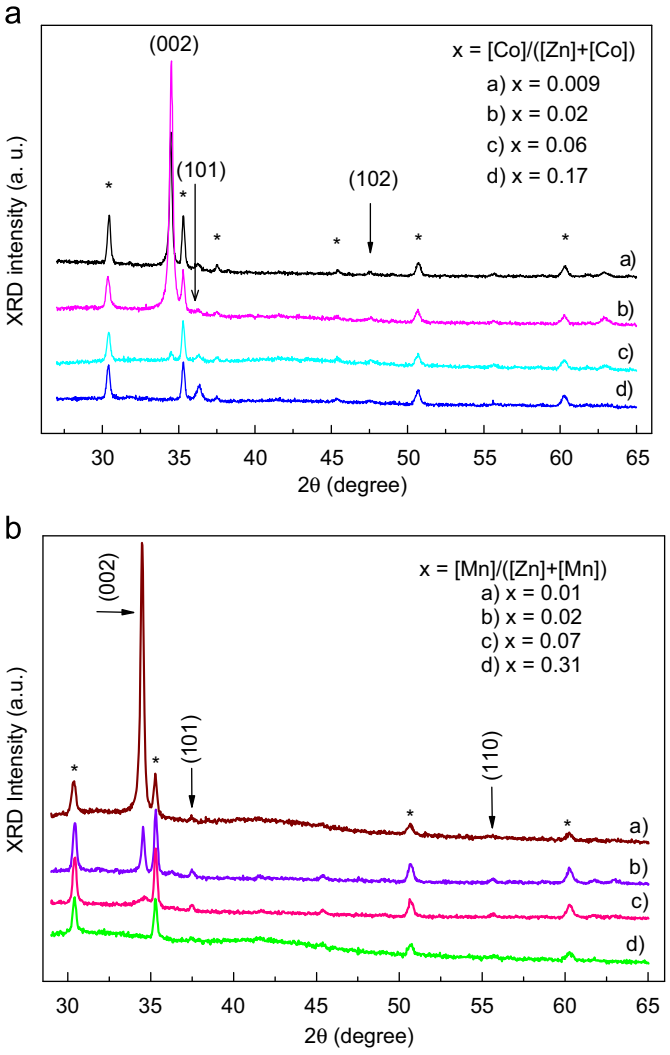

Fig. 2. (a) XRD scan diagram of $Zn_{1-x}Co_xO$ films for different Co concentrations, (b) XRD scan diagram of $Zn_{1-x}Mn_xO$ films for different Mn concentrations. (*) corresponds to XRD scan diagram of ITO substrate.

Fig. 2(a) and (b) shows the X-ray diffraction peaks for different samples of $Zn_{1-x}M_xO$ with different Co and Mn concentrations in the films, respectively. The peaks with the symbol (*) belong to the ITO substrate. In both figures the peaks placed in 34.42° and 36.25° correspond to crystallographic directions (0 0 2) and (1 0 1) of the ZnO wurtzite structure. Our $Zn_{1-x}M_xO$ thin films grow preferentially along the (0 0 2) direction but this preferential direction of growth is reduced with increasing M concentration and at concentrations above 10% the (1 0 1) direction is preferred. The wurtzite diffraction peaks disappear of the X-ray diffraction patterns for concentrations larger than 20% for Co and larger 30% for Mn in the films. It is rather curious that diffraction peaks are no longer observed for the films with the highests M concentrations, thus suggesting that these films are amorphous or strongly disordered. Therefore, we resort to the Raman spectroscopy to determine the structure of the thin films with high M concentrations.

According to group theory, cubic spinels have the following phonon modes at the Γ point [25]

$$\Gamma = A_{1g}(R) + E_g(R) + 3T_{2g}(R) + 5T_{1u}(IR) + T_{1g} + 2A_{2u} + 2E_u + 2T_{2u}$$

where R and IR corresponds to Raman- and infrared-active modes, respectively, where one triply degenerated T_{1u} correspond to

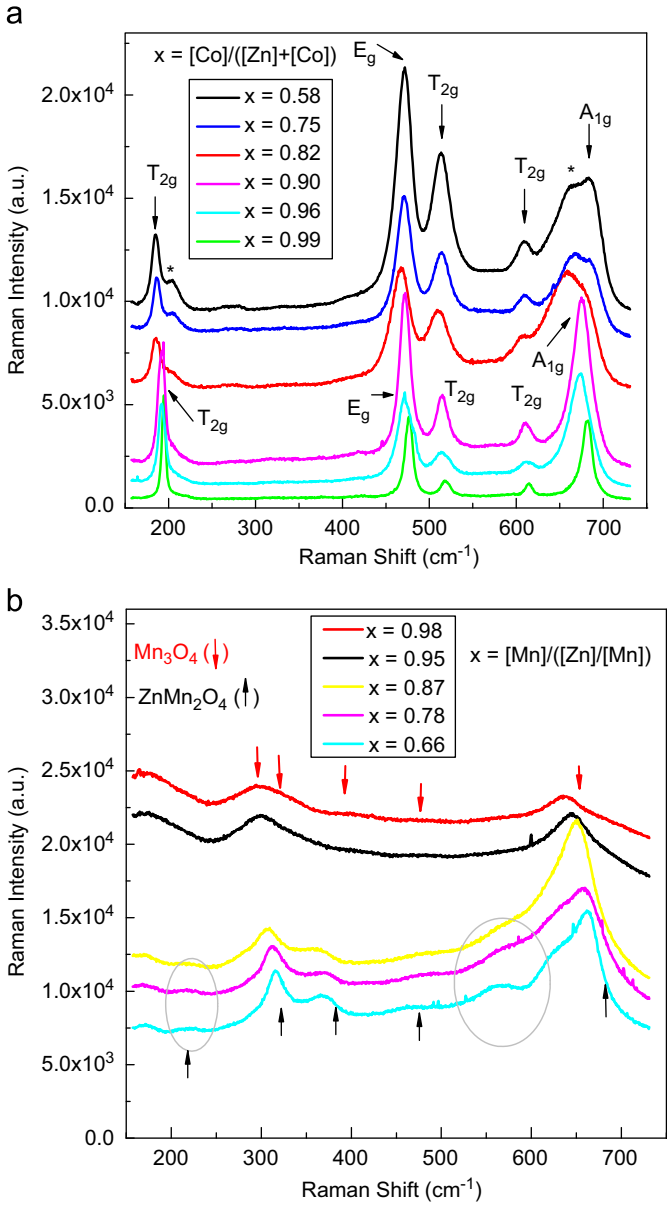

Fig. 3. (a) Raman spectra for different concentrations of Co (x=[Co]/([Zn]+[Co]) in the ZnO lattice. (b) Raman spectra for different concentrations of Mn x=[Mn]/([Zn]+[Mn]) in the ZnO lattice.

acoustic modes, and T_{1g}, E_u, A_{2u}, and T_{2u} are silent modes. Therefore, five Raman-active modes are expected in this structure. Fig 3(a) and (b) shows the results of different Raman spectra for samples with high Co and Mn concentrations, respectively. Fig 3(a) exhibits two different types of Raman spectra that can be related to two different compounds, namely the $ZnCo_2O_4$ and the Co_3O_4 spinels. For Co concentrations in the films higher than 90% five narrow Raman modes are appreciated whose frequencies match with the Raman-active modes of the pure Co_3O_4 spinel as reported in the literature [26] (see values in Table 1). The small frequency changes between our samples and those reported in the literature are probably due to the Zn impurities present in our samples.

For Co concentrations below 90% the Raman spectra is formally identical to the $ZnCo_2O_4$ films in phase spinel reported in the literature [27] (see Table 1). It can be observed that more than five Raman-active modes appear in the spectra. We think that the additional Raman modes [peaks marked with the asterisk in

Table 1
Frequencies and symmetries of Raman modes observed in $ZnCo_2O_4$ (x=0.58) thin films compared to those reported in the literature (Ref. 27)and of Co_3O_4 (x=0.99) thin films compared to those reported in the literature (Ref. 5).

Phonon symmetry	Frequency (cm^{-1}) $ZnCo_2O_4$ (x=0.58)	Frequency (cm^{-1}) $ZnCo_2O_4$ (Ref. 27)	Frequency (cm^{-1}) Co_3O_4 (x=0.99)	Frequency (cm^{-1}) Co_3O_4 (Ref. 5)
T_{2g}	193	193	193	194.4
E_g	476	476	476	482.4
T_{2g}	517	517	517	521.6
T_{2g}	615	615	615	618.4
A_{1g}	683	683	683	691.0
*	204	200		
*	661	660		

Fig. 3(a) and Table 1] are additional modes that appear due to the inversion of spinels. The mixture of cations in both crystal positions can produce the splitting of Raman modes to a higher or lower frequency depending on the contribution of the cations to each Raman mode and the mass of each cation. In particular, the Raman T_{2g} mode with the lowest frequency around 193 cm^{-1} in Co_3O_4 splits into two modes at 185 and 204 cm^{-1} in $ZnCo_2O_4$. The mode at 193 cm^{-1} is a A–O stretching mode in AB_2O_4 spinels which is mainly contributed only by Co ions in tetrahedral position in Co_3O_4 [28]. Therefore, one can understand that the mode at 185 cm^{-1} in $ZnCo_2O_4$ is due to the occupation of tetrahedral sites by Zn, which has a slightly larger mass than Co, and that the 204 cm^{-1} mode is a signature of residual Co atoms in the tetrahedral sites. Contrarily, the Raman A_{1g} mode with the highest frequency around 682 cm^{-1} in Co_3O_4 splits into two modes at 661 and 686 cm^{-1} in $ZnCo_2O_4$. Since the A_{1g} mode is a B-O stretching mode in AB_2O_4 spinels which is mainly contributed by the Co in octahedral coordination in Co_3O_4 [28], the mode at 686 cm^{-1} in $ZnCo_2O_4$ indicates the presence of Co in octahedral coordination while the mode at 661 cm^{-1} evidences the presence of a considerable amount of Zn ions in octahedral coordination.

As already commented, manganese oxide spinels (AMn_2O_4) typically have tetragonal spinel structure [29]. According to group theory, tetragonal spinels have the following phonon modes at the Γ point [30]

$$\Gamma = 2A_{1g}(R)+3B_{1g}(R)+B_{2g}(R)+4E_g(R)+5A_{2u}(IR)+7E_u(IR)+2A_{1u}+A_{2g}+2B_{2u}$$

where R and IR corresponds to Raman- and infrared-active modes, respectively, where one A_{2u} and one double degenerate E_u correspond to acoustic modes, and A_{1u}, A_{2g}, and B_{2u} are silent modes. Therefore, 10 Raman-active modes are expected in this structure. Fig 3(b) displays the Raman spectra for different samples with high Mn concentrations. It is observed that the Raman spectra can be classified again into two different classes. The first type of Raman spectra occurs for molar fractions of Mn between 66 and 78% and they correspond to a mixed spinel structure of $ZnMn_2O_4$ with tetragonal symmetry since similar bands to ours have been reported by Malavasi et al. [28] and summarized in Table 2. Black upward arrows in Fig. 3(b) mark the frequencies of the Raman modes of $ZnMn_2O_4$ reported by Malavasi et al. for comparison with our spectra [28]. Fig 4(a) shows a decomposition of the Raman spectrum of $ZnMn_2O_4$ assuming that this stoichiometry is close to our sample with x=0.66. We have fitted up to 8 peaks out of the 10 allowed Raman modes, whose frequencies compare reasonably with those of the five peaks reported in Ref. 28. Note that the frequencies of our $ZnMn_2O_4$ samples can be considerably affected by lack of stoichiometry. In fact, it can be observed that there is a shift of the

Table 2
Frequencies and symmetries of Raman modes observed in $ZnMn_2O_4$ (x=0.66) and of Mn_3O_4 (x=0.95) thin films compared to those reported in the literature (Ref. 28).

Phonon mode	Frequency (cm^{-1}) $ZnMn_2O_4$ (x=0.66)	Frequency (cm^{-1}) $ZnMn_2O_4$ (Ref. 28)	Frequency (cm^{-1}) Mn_3O_4 (x=0.95)	Frequency (cm^{-1}) Mn_3O_4 (Ref. 28)
Peak 1	276	300.2	278	
Peak 2	316	320.5	301	290
Peak 3	320		334	319
Peak 4	369	381.9	405	374
Peak 5	463	475.5	474	479
Peak 6	563		599	
Peak 7	630			
Peak 8	663	677.6	645	660

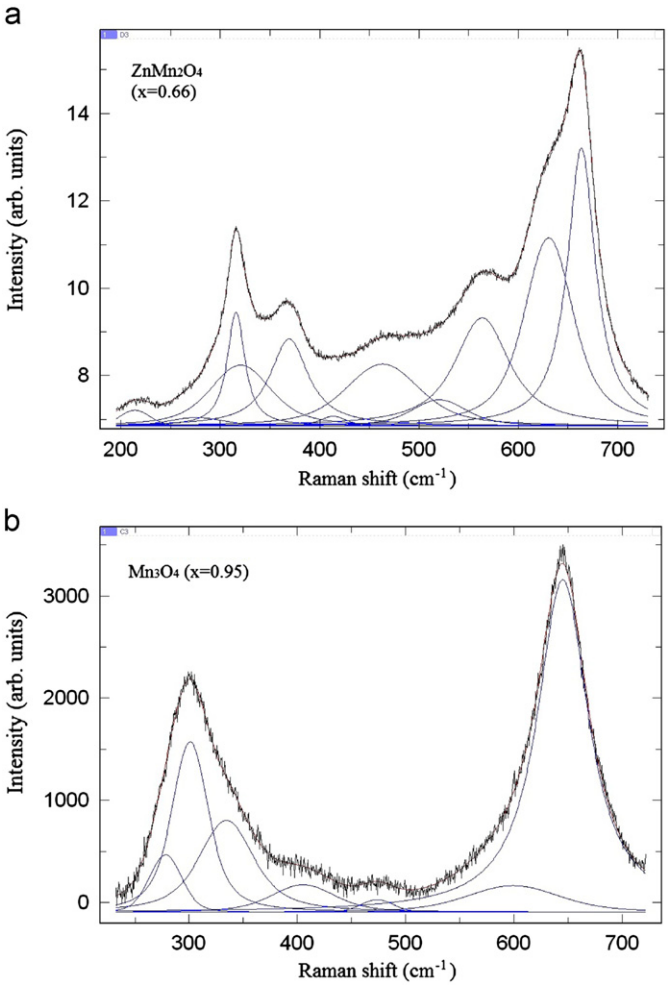

Fig. 4. (a) Raman spectra of a sample with a Mn molar fraction of 0.66 ($ZnMn_2O_4$) decomposed into Gaussian profiles. (b) Raman spectra of a sample with a Mn molar fraction of 0.95 (Mn_3O_4) decomposed into Gaussian profiles.

Raman modes for higher Mn concentrations and that our frequencies are shifted with respect to those reported by Malavasi et al. [28] thus suggesting that our samples with $x > 0.66$ have an excess of Mn with respect to the $ZnMn_2O_4$ stoichiometry.

The second class of Raman spectra correspond to the three samples with Mn molar fraction above x=0.85 in the films where the Raman spectrum is dominated by two wide bands. We have ascribed this sample to the spinel Mn_3O_4. Fig 4(b) shows a decomposition of the Raman spectrum of Mn_3O_4 assuming that this stoichiometry is close to our sample with x=0.95. We have fitted up to 7 peaks out of the 10 allowed Raman modes, whose frequencies compare reasonably with those of the five peaks reported in Ref. 28 for Mn_3O_4. In Fig. 3(b), we have marked with red downward arrows the frequencies of the stronger bands of the Mn_3O_4 spinel reported by Lutz et al. and Malavasi et al. [28,31]. The frequencies of the Raman bands observed in our films with the highest Mn concentration match reasonably with the frequencies of the Raman bands observed by other authors (see Table 2). Note that in our Mn_3O_4 films the fourth and five peaks reported by Malavasy et al. are observed as a broad band ranging from 250 to 350 cm^{-1} where three Gaussians can be fitted around 278, 301 and 334 cm^{-1}. Similarly, the broad band ranging from 520 to 700 cm^{-1} in our films has been fitted to two Gaussian profiles, being the stronger in intensity at a frequency of 645 cm^{-1}, which is close to the value reported for the strongest Raman peak of Mn_3O_4 (660 cm^{-1}).

Finally, we want to stress that the strongly broadened Raman bands of the films with the highest Mn concentrations suggest the formation of strongly deformed or amorphous structures of tetragonal Mn_3O_4 spinel as compared to the narrow peaks reported in Ref. 28. However, we are confident that our films with the highest Mn concentrations correspond to the Mn_3O_4 spinel because the magnetization curves that have been measured in our previous work exhibit the same magnetization properties than Mn_3O_4 spinel [32].

4. Conclusions

Spinel-type ZnM_2O_4 and M_3O_4 (M=Mn, Co) thin films have been obtained by electrodeposition with high transparency and homogeneity. EDS results confirm the incorporation of the Co or Mn ions in the ZnO lattice. Up to 20% at. Co and 10% at. Mn can be incorporated into the wurtzite ZnO lattice, whereas above those limits spinel-type compounds are formed as evidenced by Raman scattering measurements. At intermediate M concentrations in the initial solution spinel-type ZnM_2O_4 is formed. At higher M concentrations pure Co_3O_4 spinel is formed while a very deformed spinel or an amorphous material is obtained in the case of Mn_3O_4.

Acknowledgements

This work was supported by Spanish Government through MICINN grants MAT2009-14625-C03-03, MAT2010-21270-C04-04 and MALTA CSD2007-0045. Financial support by the European Commission through NanoCIS project (PIRSES-GA-2010-269279) is gratefully acknowledged. Finally, we also want to acknowledge the support of Vicerrectorado de Investigación y Desarrollo de la Universitat Politècnica de València through projects UPV2011-0914 PAID-05-11 and UPV2011-0966 PAID-06-11.

References

[1] J. Ghose, K.S.R.C. Murthy, J. Catal. 162 (1996) 359.
[2] N. Guilhaume, M. Primet, J. Chem. Soc. Faraday Trans. 90 (1994) 1541.
[3] B.L. Yang, D.S. Chen, S.B. Lee, Appl. Catal. 70 (1991) 161.

[4] J.P. Jacobs, A. Maltha, J.G.H. Reinthjes, J. Drimal, V. Ponec, H.H. Brongersma, J. Catal. 147 (1994) 294.
[5] J. Sloczynski, J. Ziólkovski, B. Grzybowska, R. Grabowski, D. Jachewicz, K. Wcislo, L. Gengembre, J. Catal. 187 (1999) 410.
[6] X. Niu, W.P. Du, W.M. Du, Sens. Actuators B 99 (2004) 405.
[7] C. Ai, M. Yin, C. Wang, J. Sun, J. Mat. Sci. 39 (2004) 1077.
[8] Y. Sharma, N. Sharma, G.V. Subba Rao, B.V.R. Chowdari, Adv. Funct. Mat. 17 (2007) 2855.
[9] W.M. Shaheen, A.A. Ali, Mater. Res. Bull. 36 (2001) 1703.
[10] D. Jarosch, Mineral. Petrol. 37 (1987) 15.
[11] C. Otero Areán, M. Peñarroya Mentruit, A.J. López López, J.B. Barra, Phys. Eng. Aspects 180 (2001) 253.
[12] A. Manthiram, J. Kim, Chem. Mater. 10 (1998) 2895.
[13] K.L. Zhang, J.B. Yuan, G.F. Zhu, Q.C. Zhang, J.T. Tang, J. Wuhan Univ.(Nat. Sci. Ed.) 4 (1997) 428.
[14] A.G. Shi, A.H. Hang, J. Fang, J.S. Chi, M.M. Wu, Chin. J.Inorg. Chem. Ind. 5 (2001) 14.
[15] K.J. Omata, T.K.S. Takada, S.J. Kasahara, M.N.Y.S. Yamada, Appl. Catal. A:Gen. 146 (1996) 255.
[16] B. Chi, J. Li, X. Yang, H. Lin, N. Wang, Electrochim. Acta 50 (2005) 2059.
[17] X. Wei, D. Chen, W. Tang, Mat. Chem. Phys. 103 (2007) 54.
[18] S. Trasatti, G. Lodi, Electrodes of Conductive Metallic Oxides, Part A, in: S. Trasatti (Ed.), Elsevier, Amsterdam, 1980. in:.
[19] P. Rasiyah, A.C.C. Tseung, D.B. Hibbert, J. Electrochem. Soc.: Electrochem. Sci. Techhol. 129 (1982) 1724.
[20] R.N. Singh, J.F. Koenig, G. Poillerat, P. Chartier, J. Electrochem. Soc. 137 (1990) 1408.
[21] M. Tortosa, M. Mollar, B. Marí, J. Cryst. Growth 304 (2007) 97.
[22] M. Tortosa, M. Mollar, B. Marí, Phys. Status Solidi C 5 (2008) 3467.
[23] B. Marí, J. Cembrero, M. Mollar, M. Tortosa, Phys. Status Solidi C 5 (2008) 555.
[24] M. Tortosa, M. Mollar, B. Marí, F. Lloret, J. Appl. Phys. 104 (2008) 033901.
[25] A. Chopelas, A. Hofmeister, Phys. Chem. Miner. 18 (1991) 279.
[26] V.G. Hadjiev, M.N. Iliev, I.V. Vergilov, J. Phys. C: Solid State Phys. 21 (1988) 199.
[27] K. Samanta, P. Bhattacharya, R.S. Katiyar, W. Iwamoto, P.G. Pagliuso, C. Rettori, Phys. Rev. B 73 (2006) 245213.
[28] L. Malavasi, P. Galinetto, M.C. Mozzati, C.B. Azzoni, G. Flor, Phys. Chem. Chem. Phys. 4 (2002) 3876.
[29] M. Nogues, P. Poix, Ann. Chim. (Paris) 1972 (1972) 301.
[30] Bilbao Crystallographic Server, 〈http://www.cryst.ehu.es〉.
[31] H.D. Lutz, B. Müller, H.J. Steiner, J. Solid State Chem. 90 (1991) 54.
[32] M. Mollar, M. Tortosa, R. Casasús, B. Marí, Microelectron. J. 40 (2009) 276–279.